Journal of Nano- and Electronic Physics
Vol. **12** No 4, 04015(5pp) (2020)

Журнал нано- та електронної фізики
Том **12** № 4, 04015(5cc) (2020)

Effect of Weak Confinement on the Optical Properties of Chemically Synthesized ZnS Nanoparticles

K.C. Handique*, P.K. Kalita

Rajiv Gandhi University, Department of Physics, Itanagar 791112, Arunachal Pradesh, India

(Received 12 April 2020; revised manuscript received 20 August 2020; published online 25 August 2020)

Zinc sulphide nanostructures have been synthesized with different compositions of Zn/S ratio through chemical route. The XRD shows polycrystalline hexagonal structure for all the samples. The W-H plot shows particle sizes in the range 29.54 nm to 41.36 nm and strain from 0.021 to 0.026. A larger particle size supports weak quantum confinement in the samples. No significant increase in the band gap was found from the optical studies. Using one-dimensional weak confinement model, transition levels for defect emission in the visible region are obtained.

Keywords: ZnS nanostructure, Weak confinement, W-H plot, PL spectra, Defect induced emission.

DOI: 10.21272/jnep.12(4).04015 PACS numbers: 78.67.Bf, 81.07.Bc

1. INTRODUCTION

Zinc sulphide (ZnS) is one of the most important II-VI binary composite materials for its potential candidature in various optoelectronic applications such as electroluminescence devices, photonic devices, field emission devices, nonlinear optical devices, gas and UV sensors, biological as well as photonic devices [1-3]. It has been attracting considerable attention due to its excellent optoelectronic properties along with reasonably high optical absorption coefficient, transmittance, refractive index, antireflection and work function [4, 5]. Non-toxicity is another important factor making this nanomaterial relevant for the fabrication of high performance sensors [6], lasers [7] and different infrared applications. Moreover, chemical bath deposition (CBD) is a versatile and efficient technique for synthesizing nanosized materials nowadays, as it requires relatively non-sophisticated equipment, low temperature and simple implementation [8, 9]. A comprehensive review on the development of ZnS nanostructures using various techniques other than CBD can be seen elsewhere such as chemical vapor deposition [10], atomic layer deposition [11], radio frequency magnetic sputtering [12] etc. Some of studies performed on ZnS nanoparticles carried out through CBD technique can be found where focuses were given on improvement of the quality of the material by manipulating various parameters like reaction time, bath temperature, concentration of the reagents etc. [13-16]. Although all of them try to optimize various growth parameters differently to improve properties of ZnS nanoparticles, their way of doing, the use of reagents and other environmental factors differ significantly. Sometimes it seems difficult to obtain the same properties on the synthesized materials with repetition of earlier accepted growth conditions, as it is not so easy to take care for all the factors involved in the overall synthesis procedure. As a result, this variation still makes the production of a proper good quality ZnS material with a single set of parameters and reagents used in the synthesis lags behind. Thus, a proper, systematic and monotonous study on the synthesis of ZnS nanostructures for confident and fruitful application in various fields cannot be denied. With these prospects, we have attempted to make a little contribution towards this area by synthesizing and analyzing ZnS nanostructures by varying the ratio of their constituent complexes and some surrounding conditions. Thus, in this work we are to determine the best ratio of zinc and sulphur containing complexes in a particular range of bath temperatures. From the structural and morphological point of view, a perfect crystal does not exist in real life. While characterizing the nanostructures, for accurate and reliable calculation of the particle size of the crystallites, Williamson-Hall (W-H) plot technique is highly preferred and dominant one. The deviation of the crystallite sizes of the nanoparticles leads to broadening of the diffraction peaks. In W-H plot, microstrain present in a crystal is also taken into consideration while determining the crystallite size. Strain can be realized as a measure of the distribution of lattice constants due the crystal imperfections arising in a crystal such as lattice dislocations, grain boundary triple junctions, stacking faults etc. [17]. The crystallite size varies with peak broadening as $1/\cos\theta$ whereas the strain varies with $\tan\theta$ and this difference makes us able to discriminate the effects of size and strain on peak broadening. As the Williamson-Hall (W-H) plot analysis method holds a dominant position till date in determining the crystallite size and strain, we have used this technique to study the effects of structural parameters and their changes on the optical properties of the synthesized samples.

2. EXPERIMENTAL

2.1 Materials Used

All the materials required in the synthesis are used as received from Merck without any further purification. Materials used are zinc acetate, sodium sulphide, polyvinyl pyrrolidone (PVP), and ammonia solutions along with deionized water. The pH value and molar concentration of the samples are kept at 10 and 0.5 M, respectively, for all synthesizes.

* kshirud.handique@rgu.ac.in

2.2 Synthesis of ZnS Nanoparticles

Initially 3 % PVP solution is prepared by dissolving 3 mg PVP in 100 ml deionized water and 25 ml of zinc acetate is added to it. 2-3 drops of ammonia solution are added to the mixture to maintain the pH level. The whole system is kept on a magnetic stirrer at 1500 rpm and a temperature of 50 °C. 25 ml of sodium sulphide solution which is also dissolved in 3 % PVP solution is slowly added to the mixture and stirred for 1 h to get 1:1(S1) homogeneous solution. Other two samples, S2 and S3, are also synthesized in the same manner by keeping the ratio of zinc acetate and sodium sulphide as 1:2 and 1:3, respectively.

For characterization, X-ray diffraction is performed on the samples with a Rigaku Ultima IV diffractometer. Phase and crystal structures are determined from the XRD peaks. CuKα radiation is used in all the slits. The current and generator tension have been kept at 40 mA and 40 kV, respectively. XRD for all the samples is done in continuous scan mode for the purpose of comparison. Optical absorption of the samples was done using an Agilant Technologies Cary 60 UV-Vis spectrometer with the range from 800 nm to 300 nm. All the spectra were corrected for baseline. Photoluminescence measurements were performed with a Cary Eclipse fluorescence spectrometer.

3. RESULTS AND DISCUSSION

3.1 X-Ray Diffraction Analysis

X-ray diffraction is one of the most powerful tool for structural characterization of nanomaterials till date. It has been done on the as-synthesized samples after converting them to the powder form with the help of a PR-24 centrifuge and an ordinary oven at the scanning range of 2θ equal to 20° to 70°. The XRD spectra of the samples reveal their hexagonal wurtzite phase confirmed after comparison with the standard JCPDS data as shown in Fig. 1 (JCPDS cad no. 39-1363).

Table 1 – Structural parameters of S1, S2 and S3

Samples	(hkl)	Lattice parameters (nm)	V (nm^3)	$\cos\theta$
S1	002 104	$a = 0.3506$ $c = 0.5726$	0.0609	0.9045
S2	002 104	$a = 0.334$ $c = 0.545$	0.0526	0.9045
S3	002 104	$a = 0.3868$ $c = 0.6318$	0.0818	0.8718

The planes (002), (104), (101), (106), (102), (103) and (112) are present in S1 while (102) plane is not reflected in the spectra of S2 and (001) plane appears in case of S3. The structural parameters viz. lattice parameter, unit cell volume and interplanar angle $\cos\phi$ for all the three samples are calculated by using the following set of equations and presented in Table 1:

$$a = d\sqrt{h^2 + k^2 + l^2}\,, \tag{3.0}$$

$$\frac{c}{a} = 1.633\,, \tag{3.1}$$

$$V = \frac{\sqrt{3}}{2}a^2 c\,, \tag{3.2}$$

$$\cos\phi = \frac{h_1k_1 + k_1k_2 + \frac{1}{2}(h_1k_2 + h_2k_1) + \frac{3a^2}{4c^2}}{\sqrt{\left(h_1^2 + k_1^2 + h_1k_1 + \frac{3a^2}{c^2}l_1^2\right)\left(h_2^2 + k_2^2 + h_2k_2 + \frac{3a^2}{c^2}l_2^2\right)}} \tag{3.3}$$

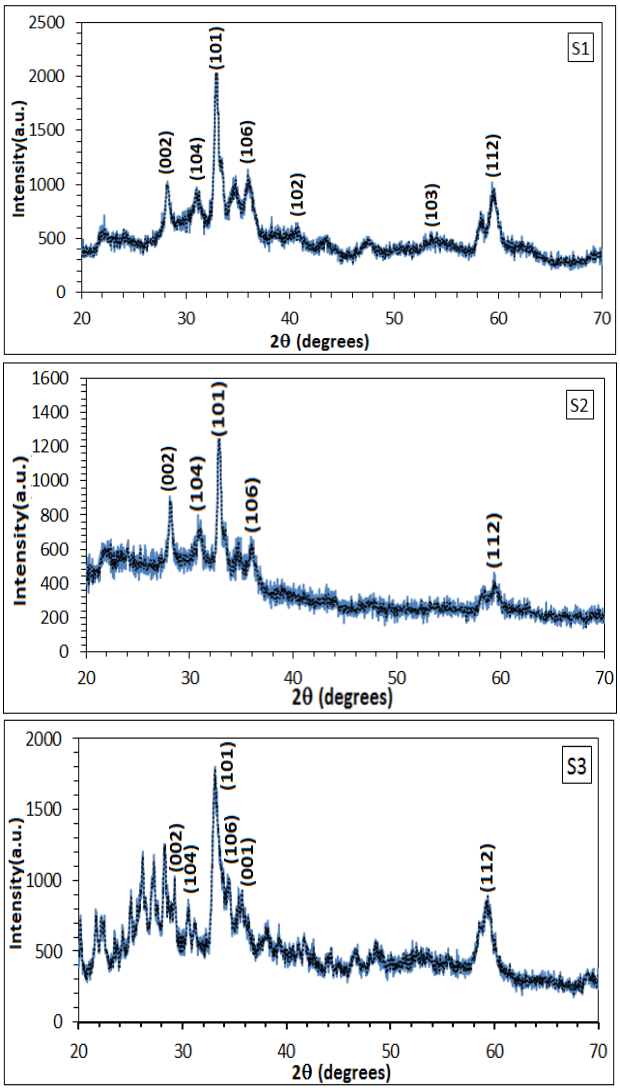

Fig. 1 – X-ray diffraction spectra of S1, S2 and S3

The lattice parameters are calculated by taking the (002) dominating plane in all the three samples and are found to agree well with the standard one. The unit cell volume of S2 is slightly greater than S1 which indicates that in sample S2 the surface is well modified that may reduce the possibility of non-radiating recombination processes on the nanocrystals. In case of S3, the unit cell volume increases again which means that the surface of the nanocrystal is not well modified as in case of S2 where the possibility of eliminating the non-radiative recombination paths is less. Thus, the ratio 1:2 of the constituent ion complexes is highly efficient from the structural point of view. The interplanar angles of the samples are calculated by taking (002) and (104) planes

which appear consecutively in all the three samples. The value of $\cos\phi$ is almost the same for S1 and S2 but it slightly decreases in case of S3 which may be due to the presence of low compressive strain in the crystals.

3.2 W-H Plot Analysis

As already mentioned, the microstrain present in a crystal is an indispensable part in determining the crystallite size which varies with $\tan\theta$ whereas in the Scherrer formula the overall crystallite size varies with $\cos\theta$. Here, W-H plot has been presented as shown in Fig. 2 by using the uniform deformation model (UDM). Combining Scherrer equation and the expression for microstrain (ε) leads to

$$\beta_{hkl}\cos\theta = \frac{k\lambda}{D} + 4\in\sin\theta\,. \qquad (3.4)$$

The above equation is according to UDM formulation [17, 18]. W-H plot has been presented by plotting $\beta\cos\theta$ vs $4\sin\theta$ along with the strain and particle size. The Y-intercepts and slopes of the fitted curves represent the crystallite size and strain, respectively. A detailed quantitative assessment of the strain and particle size is presented in Table 2.

Table 2 – Structural parameters of the samples

Samples	Size (nm)	Strain	Dislocation density (m^{-2})	Bond length (nm)
S1	41.36	0.026	2.17×10^{16}	0.042
S2	29.54	0.021	2.58×10^{16}	0.0381
S3	35.30	0.023	1.63×10^{16}	0.0511

The W-H plots show tensile strain for all the three samples S1, S2 and S3. The strain is deeply related to the bond length between zinc and sulphide in this II-VI binary chalcogenide as strain induced deformations can change the bonding patterns among the individual atoms.

The bond length between zinc and sulphur has also been calculated using Eq. (3.5) and presented in Table 2.

$$L = [0.3a^2 + (0.5-u)^2c^2]\,, \qquad (3.5)$$

where a and c are the lattice constants of ZnS nanoparticles, u is the internal parameter which can be given as

$$u = \frac{a^2}{3c^2} + 0.25\,.$$

3.3 UV-Vis and PL Analysis

UV-Vis spectroscopy has been performed on the samples with scanning range 300 to 800 nm. All the three samples show small blue shift as seen from Tauc plots which may be due to the weak quantum confinement. PVP plays the role of providing quantum confinement. The band gaps of the prepared samples have been estimated from Tauc plots as shown in Fig. 3. A small increment in band gap as shown in Table 3 for all samples suggests weak quantum size effect.

The photoluminescence spectra of the synthesized samples are done with the scanning range of 250 nm to 550 nm as shown in Fig. 4. Excitation wavelength is taken around 325 nm for all the samples. The photolu-

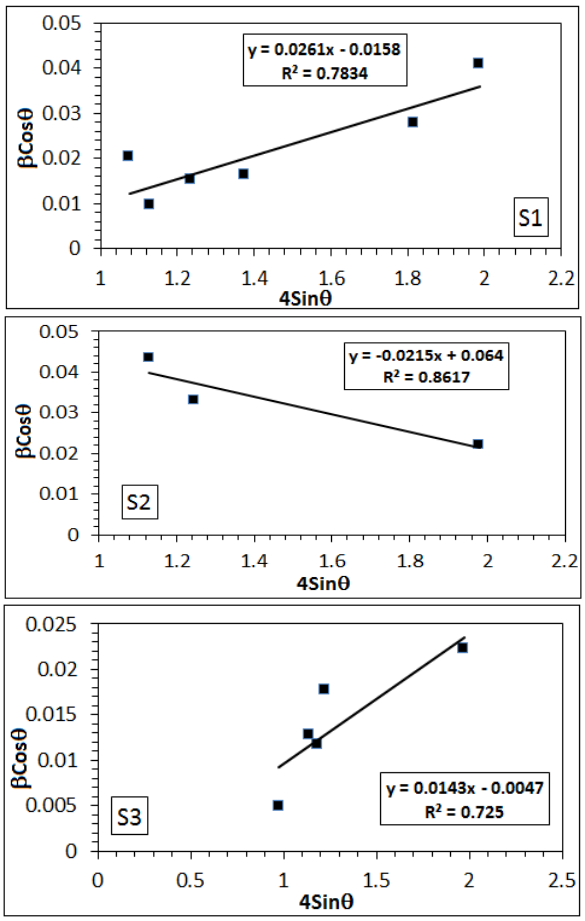

Fig. 2 – W-H plots of S1, S2 and S3

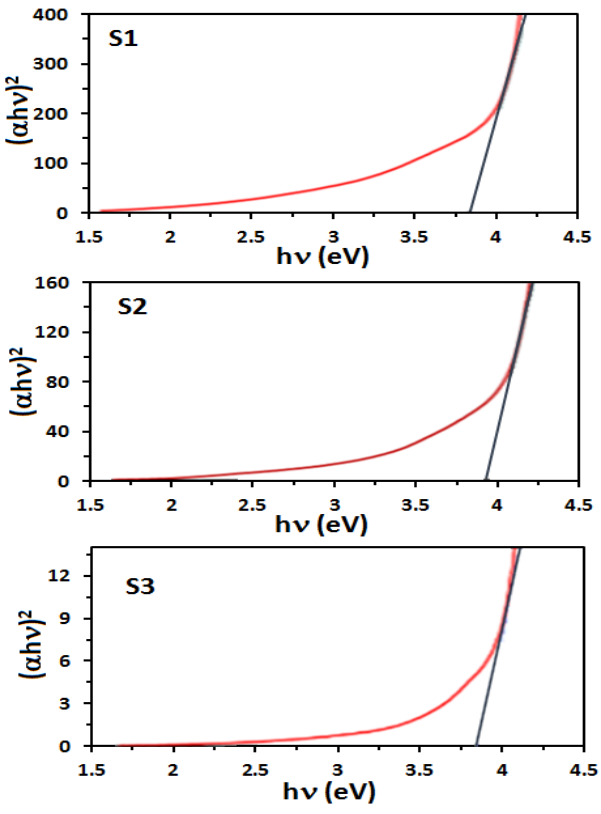

Fig. 3 – Tauc plots of the samples

Table 3 – Optical parameters of S1, S2 and S3

Samples	λ_{nbe} (nm)	Intensity (a.u.)	Band gap (eV)
S1	417	146	3.8
S2	420	220	3.9
S3	415	70	3.85

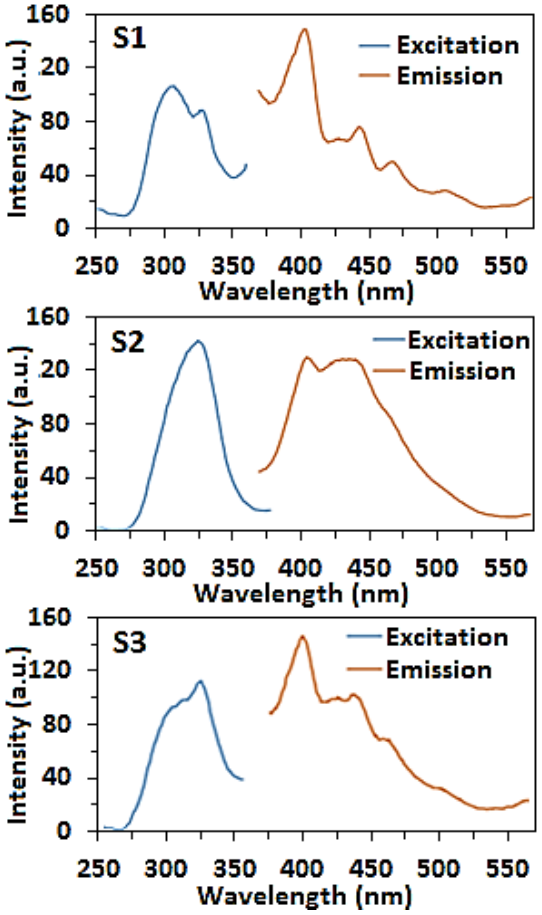

Fig. 4 – PL spectra of S1, S2 and S3

minescence spectra of the prepared samples clearly reflect their optoelectronic properties through their recombination kinetics. Considering the one-dimensional model as suggested by Pijus Kanti Samanta et al. [19], the various transition levels corresponding to the emission in the visible region can be estimated. The energy gap for transition $n \to 1$ in the weak confinement regime is approximately given by Eq. (3.6)

$$\Delta E_{n-1} = \frac{h^2}{8MR^2}(n^2-1) = \frac{\alpha}{2}(n^2-1)\,. \qquad (3.6)$$

Here $\alpha = h^2/8MR^2 = 0.000222534$ eV, 0.00365139 eV and 0.0019695 eV for S1, S2 and S3, respectively, M is the total mass of the electron-hole system given by $M = me^* + mh^*$ and R is the radius of the nanoparticles. The estimated particle size from W-H plot has been used to find out the value of alpha for three samples. The transition levels are expected to be controlled by the particle size. The PL emission peaks in the visible region and their corresponding energy and the transition levels are estimated from the above equation and are shown in Table 4.

The transition level from the excited state to the ground state as a function of wavelength is illustrated in Fig. 5, which shows lowering of transition levels with increasing wavelength.

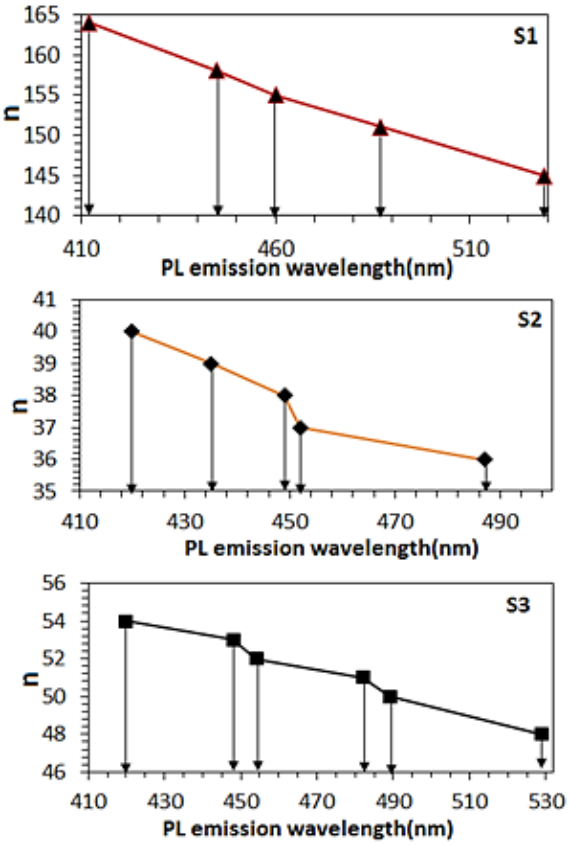

Fig. 5 – Transitions corresponding to impurity emission

Table 4 – PL emission peaks and corresponding transition levels

Samples	Wavelength (nm)	Energy (eV)	n
S1	412	3.0097	164
	445	2.7865	158
	460	2.6956	155
	487	2.5462	151
	529	2.3440	145
S2	420	2.9523	40
	435	2.8505	39
	449	2.7616	38
	452	2.7430	37
	487	2.5462	36
S3	420	2.9523	54
	448	2.7678	53
	454	2.7312	52
	482	2.5726	51
	489	2.5357	50
	529	2.3440	48

4. CONCLUSIONS

Zinc sulphide nanostructures have been synthesized with different compositions of zinc and sulphur complexes through chemical route. Three samples are prepared by mixing their constituent zinc and sulphur containing complexes at the ratio of 1:1, 1:2 and 1:3, respec-

tively. The XRD shows polycrystalline hexagonal structure for all the samples. From the W-H plot, the particle size and strain have been calculated. A larger particle size supports weak quantum confinement in the samples. Other structural parameters viz. dislocation density, bond length are also estimated which shows a slight variation with respect to the compositional variation. The optical studies also confirmed a weak confinement because of small blue shift and hence no significant increase in band gap. Using one-dimensional weak confinement model, transition levels for defect emission in the visible region are found to be within 435 nm to 529 nm. Hence, it is inferred that defect emission predominantly governs the luminescence in weakly confined zinc sulphide nanoparticles.

ACKNOWLEDGEMENTS

The authors wish to sincerely thank faculty in charge, department of Physics, Nerist for providing XRD facility and department of chemistry, Rajiv Gandhi University for providing spectrometric facilities.

REFERENCES

1. R. Zein, I. Alghoraibi, *Int. J. Chem Tech. Res.* **6**, 3220 (2014).
2. X.S. Fang, Y. Bando, G.Z. Shen, C.H. Ye, U.K. Gautam, P.MFJ Costa, C.Y. Zhi, C.C. Tang, D. Golberg, *Adv. Mater.* **19**, 2593 (2007).
3. X.S. Fang, U.K. Gautam, Y. Bando, B. Dierre, T. Sekiguchi, D. Golberg, *J. Phys. Chem. C* **112**, 4735 (2008).
4. T.B. Nars, N. Kamoun, M. Kazanri, R. Bennaceur, *Thin Solid Films* **4**, 500 (2006).
5. A. Antony, K.V. Murali, R. Manoj, M.K. Jayaraj, *Mater. Chem. Phys.* **90**, 106 (2005).
6. X.S. Fang, Y. Bando, M.Y. Liao, U.K. Gautam, C.Y. Zhi, B. Dierre, *Adv. Mater.* **21**, 2034 (2009).
7. R.H. Page, K.I. Schaffers, L.D. DeLoach, G.D. Wilke, F.D. Patel, J.B. Tassano, S.A. Payne, W.F. Krupke, A. Burger, *IEEE J. Quantum. Elect.* **33**, 609 (1997).
8. S.M. Pawar, B.S. Pawar, J.H. Kim, Oh-Shim Joo, C.D. Lokhande, *Curr. Appl. Phys.* **11**, 117 (2011).
9. I.J. Gonzalez-Chan, I.J. Gonz´alez-Panzo, A.I. Oliva, *J. Electrochem. Soc.* **164**, D95 (2017).
10. J. Hu, G. Wang, C. Guo, D. Li, L. Zhang, J. Zhao, *J. Lumin.* **122**, 172 (2007).
11. J. Kuhs, T. Dobbelaere, Z. Hens, C. Detavernier, *J. Vac. Sci. Technol. A* **35**, 01B11 (2007).
12. X.J. Zheng, Y.Q. Chen, T. Zhang, B. Yang, C.B. Jiang, B. Yuan, Z. Zhu, *Sensor. Actuat. B* **147**, 442 (2010).
13. W. Vallejo, M. Hurtado, G. Gordillo, *Electrochim. Acta* **55**, 5610 (2010).
14. Limei Zhou, Nan Tang, Sumei Wu, *Surf. Coat. Tech.* **228**, S146 (2013).
15. P.U. Bhaskar, G.S. Babu, Y.B.K. Kumar, Y. Jayasree, V.S. Raja, *Mater. Chem. Phys.* **134**, 1106 (2012).
16. H. Lekiket, M.S. Aida, *Mater. Sci. Semicond. Proc.* **16**, 1753 (2013).
17. T.M.K. Thandavan, S.M.A. Gani, C.S. Wong, R. Md Nor, *J. Nondestruct. Eval.* **34**, 14 (2015).
18. A.K. Zak, et al., *Solid State Sci.* **13**, 251 (2011).
19. P.K. Samanta, P.R. Chaudhuri, *J. Opt.* **41**, 75 (2012).

Вплив слабкого обмеження на оптичні властивості хімічно синтезованих наночастинок ZnS

K.C. Handique, P.K. Kalita

Rajiv Gandhi University, Department of Physics, Itanagar 791112, Arunachal Pradesh, India

Наноструктури сульфіду цинку були синтезовані хімічним шляхом для різних складів співвідношення Zn/S. XRD дослідження виявило полікристалічну гексагональну структуру для всіх зразків. Діаграма W-H показує розміри частинок в діапазоні від 29,54 нм до 41,36 нм і деформації від 0,021 до 0,026. Більший розмір частинок підтримує слабке квантове обмеження в зразках. Оптичні дослідження не виявили значного збільшення ширини забороненої зони. Використовуючи одновимірну модель слабкого обмеження отримано рівні переходу для емісії дефектів у видиму область.

Ключові слова: Наноструктура ZnS, Слабке обмеження, Діаграма W-H, Спектр фотолюмінесценції, Емісія дефектів.